

Amplified Ca^{2+} dynamics and accelerated cell proliferation in breast cancer tissue during purinergic stimulation

Mikkel B. Henningsen¹ | Kezia McWhan¹ | Vibeke S. Dam¹ | Marco Mele² |
 Katrine R. Hauerslev³ | Ninna C. S. Voss^{1,2} | Parag D. Dabir⁴ | Eva Balling² |
 Helene L. Pedersen⁴ | Pernille Vahl⁵ | Tonje Johansen⁴ | Trine Tramm⁵ |
 Peer M. Christiansen^{2,3} | Ebbe Boedtkjer¹ 

¹Department of Biomedicine, Aarhus University, Aarhus, Denmark

²Department of Surgery, Randers Regional Hospital, Randers, Denmark

³Department of Plastic and Breast Surgery, Aarhus University Hospital, Aarhus, Denmark

⁴Department on Pathology, Randers Regional Hospital, Randers, Denmark

⁵Department of Pathology, Aarhus University Hospital, Aarhus, Denmark

Correspondence

Ebbe Boedtkjer, Department of Biomedicine, Aarhus University, Hoegh-Guldborgs Gade 10, DK-8000 Aarhus C, Denmark.
 Email: eb@biomed.au.dk

Funding information

Det Frie Forskningsråd, Grant/Award Number: 7025-00050B; Kræftens Bekæmpelse, Grant/Award Numbers: R127-A8262-15-S7, R146-A9461

Abstract

Intracellular Ca^{2+} dynamics shape malignant behaviors of cancer cells. Whereas previous studies focused on cultured cancer cells, we here used breast organoids and colonic crypts freshly isolated from human and murine surgical biopsies. We performed fluorescence microscopy to evaluate intracellular Ca^{2+} concentrations in breast and colon cancer tissue with preferential focus on intracellular Ca^{2+} release in response to purinergic and cholinergic stimuli. Inhibition of the sarco-/endoplasmic reticulum Ca^{2+} ATPase with cyclopiazonic acid elicited larger Ca^{2+} responses in breast cancer tissue, but not in colon cancer tissue, relative to respective normal tissue. The resting intracellular Ca^{2+} concentration was elevated, and ATP, UTP and acetylcholine induced strongly augmented intracellular Ca^{2+} responses in breast cancer tissue compared with normal breast tissue. In contrast, resting intracellular Ca^{2+} levels and acetylcholine-induced increases in intracellular Ca^{2+} concentrations were unaffected and ATP- and UTP-induced Ca^{2+} responses were smaller in colon cancer tissue compared with normal colon tissue. In accordance with the amplified Ca^{2+} responses, ATP and UTP substantially increased proliferative activity—evaluated by bromodeoxyuridine incorporation—in breast cancer tissue, whereas the effect was minimal in normal breast tissue. ATP caused cell death—identified with ethidium homodimer-1 staining—in breast cancer tissue only at concentrations above the expected pathophysiological range. We conclude that intracellular Ca^{2+} responses are amplified in breast cancer tissue, but not in colon cancer tissue, and that nucleotide signaling stimulates breast cancer cell proliferation within the extracellular concentration range typical for solid cancer tissue.

KEYWORDS

acetylcholine, breast cancer, colon cancer, nucleotides, SERCA

Abbreviations: ACh, acetylcholine; BrdU, bromodeoxyuridine; BzATP, benzoylbenzoyl ATP; CPA, cyclopiazonic acid; EthD-1, ethidium homodimer-1; pH_o , extracellular pH; pH_i , intracellular pH; SERCA, sarco-/endoplasmic reticulum Ca^{2+} ATPase.

Mikkel B. Henningsen, Kezia McWhan and Vibeke S. Dam have contributed equally to this study.

This is an open access article under the terms of the [Creative Commons Attribution-NonCommercial](https://creativecommons.org/licenses/by-nc/4.0/) License, which permits use, distribution and reproduction in any medium, provided the original work is properly cited and is not used for commercial purposes.

© 2022 The Authors. *International Journal of Cancer* published by John Wiley & Sons Ltd on behalf of UICC.

What's new?

Molecular mechanisms influencing intracellular Ca^{2+} dynamics are deregulated in cancer cell lines. However, many implications of deregulated Ca^{2+} signaling during carcinogenesis remain unclear. Using fresh human and murine tissue biopsies, here the authors show that resting intracellular Ca^{2+} levels, organellar Ca^{2+} storage and intracellular Ca^{2+} responses to nucleotides and cholinergic stimuli are elevated during breast, but not colon, carcinogenesis. Nucleotides stimulate proliferation in breast cancer tissue within the elevated nucleotide concentration range observed in the tumor microenvironment, whereas cell death is induced only at higher concentrations. The authors propose that amplified Ca^{2+} signals facilitate breast malignancy.

1 | INTRODUCTION

Intracellular Ca^{2+} modifies metabolism, proliferation and cell death¹⁻³ consistent with a fundamental role in cancer development and progression. The cytosolic Ca^{2+} concentration is controlled by Ca^{2+} buffers and transport across cell and organelle membranes. Individual molecular mechanisms influencing intracellular Ca^{2+} dynamics are deregulated in cancer cell lines^{4,5}—supporting the potential for therapeutic intervention—but Ca^{2+} measurements from human cancer tissue and matched normal tissue are lacking.

Organellar Ca^{2+} storage—particularly in the endoplasmic reticulum—and release in response to stimuli from the local environment are key for control of the cytosolic Ca^{2+} concentration. Protein expression data suggest that the sarco-/endoplasmic reticulum Ca^{2+} ATPase isoform 2 (SERCA2/ATP2A2) is upregulated in murine breast cancer tissue compared with normal breast tissue⁶ and in human breast cancer cell lines (MCF7, MDA-MB-231, T47D) compared with nontumorigenic MCF10A breast epithelial cells.⁷ In contrast, SERCA3/ATP2A3 appears downregulated in breast and colon cancer.⁷⁻⁹ Numerous other ion channels and transporters involved in Ca^{2+} movement across the plasmalemma (eg, plasma membrane Ca^{2+} ATPase, store-operated and voltage-gated Ca^{2+} channels) or organelle membranes (eg, mitochondrial Ca^{2+} uniporter, STIM1) also show altered expression and activity or promising therapy-relevant functional consequences in breast and colon cancer cells.¹⁰⁻¹⁴ Yet, many implications of deregulated Ca^{2+} signaling during carcinogenesis remain unclear. In the current study, we functionally assessed cellular Ca^{2+} handling and potential malignant consequences in human and murine breast and colon biopsies.

Pharmacological compounds specifically targeting cellular Ca^{2+} handling are not in routine clinical use for anti-cancer therapy. However, the SERCA inhibitor thapsigargin elevates the intracellular Ca^{2+} concentration and can induce apoptosis in breast and colorectal cancer cell lines^{15,16}; and in congruence, the thapsigargin-based prodrug mipsagargin, which is activated by prostate specific membrane antigen-mediated cleavage, has shown positive results in phase-2 clinical testing in patients with hepatocellular carcinoma.¹⁷ Inhibitors of voltage-gated Ca^{2+} channels are furthermore reported to influence breast cancer risk.⁴ Notably, several anti-cancer drugs—including taxanes and anthracyclines currently used against triple-negative

breast cancer—in addition to their classically emphasized actions also modify cellular Ca^{2+} handling.¹⁸⁻²⁰

The local microenvironment of solid tumors—including breast and colon carcinomas—differs drastically from that of corresponding normal tissue in its chemical and cellular composition. Tumor acidity and hypoxia have widespread consequences for malignant progression as they alter gene and protein expression patterns and acutely modify functional activity. The raised energy demand of cancer cells challenges intracellular ATP availability, but accelerated aerobic glycolysis typically maintains intracellular ATP concentrations in a range comparable to that of normal cells.²¹ Extracellular ATP concentrations, on the other hand, are dramatically elevated from practically undetectable levels in normal tissue to the 100 μM range in solid cancer tissue.²²⁻²⁴

Micromolar concentrations of extracellular nucleotides (eg, ATP, UTP, UDP) activate purinergic P2X and P2Y receptors in the plasma membrane with potential influences on cellular Ca^{2+} levels and phenotypic traits. Whereas the ionotropic P2X receptors are cation channels that can mediate Ca^{2+} influx from the extracellular space, the metabotropic P2Y receptors can link to second messenger-derived Ca^{2+} release from intracellular stores.^{1,25} Purinergic receptors contribute to local auto- and paracrine signaling that upon activation can induce cell death but also promote cell proliferation.¹ Moreover, purinergic signals may modify cell-cell interactions and contribute, for instance, to the lack of contact inhibition characteristic for cancer cells.²⁶ Given the discrepancies between previous studies based on cultured cells,¹ purinergic receptors cannot currently be classified as strictly pro- or anti-neoplastic. Also, malignancy-dependent changes in Ca^{2+} signaling are not restricted to purinergic receptors. For instance, cellular expression patterns and functional influences from cholinergic receptors vary between organs and dynamically during carcinogenesis,²⁷ and they are known to be involved in growth regulation of lung carcinoma cells.²⁸

The phenotypical changes occurring during cell culture and the lack of realistic cultured equivalents of normal cells have previously complicated studies of carcinogenesis. Our current experimental approach evaluates (a) epithelial organoids freshly isolated from biopsies of human and murine breast cancer and matched normal breast tissue (Figures 1A and 2A) and (b) freshly isolated crypts from human colon cancer and normal colonic mucosa (Figure 3A). In these tissue

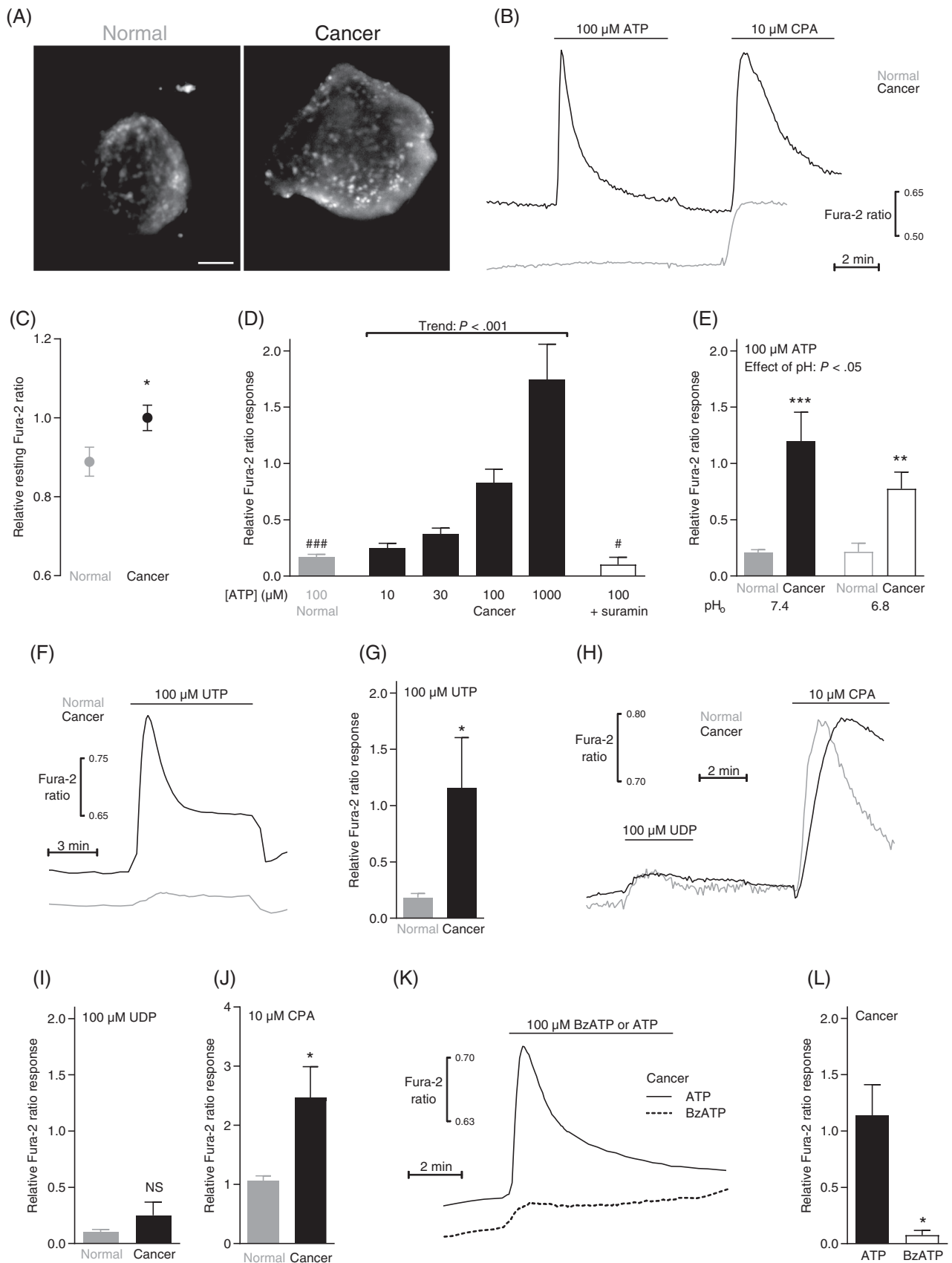


FIGURE 1 Legend on next page.

preparations, we can study ion transport across cell membranes in a realistic—yet, controllable—microenvironment and compare the mechanisms of Ca^{2+} transport among normal and cancer tissue. This is a unique approach because ion transport and specific intracellular signaling cascades in cancer cells have otherwise typically been investigated in model systems ranging from 2-dimensional monocultures to 3-dimensional homo- and heterocellular spheroids.

2 | MATERIALS AND METHODS

The present studies are based on human and murine tissue samples from colon and breast. We processed the surgical biopsies immediately after excision to isolate crypts and organoids as described below. When investigated directly after isolation—without culture—the resulting tissue preparations best preserve the functional characteristics of the breast and colon tissue.

2.1 | Human tissue

We sampled human breast cancer tissue and matched normal breast tissue as previously described in detail.^{29,30} The 33 included female patients underwent breast-conserving lumpectomy at Randers Regional Hospital or Aarhus University Hospital, Denmark, and gave written informed consent. The participants were more than 18 years of age and had tumors larger than 10 mm. Table 1 reports the clinical and pathological patient characteristics. Breast cancer was diagnosed by triple test including clinical examination, mammography combined with ultrasonography, and fine-needle aspiration cytology and/or core-needle biopsy. Two small (approximately $2 \times 2 \times 2$ mm) biopsies were sampled by the pathologist from the excised surgical specimen, one from the tumor mass and one from the macroscopically normal tissue. The biopsies immersed in cold physiological saline solution were transferred to the Department of Biomedicine at Aarhus

University, Denmark. Breast cancer malignancy was evaluated based on the Elston-Ellis modification of the Bloom-Richardson grading system.

We sampled human colon biopsies from 38 resections of biopsy-verified colon adenocarcinomas at Randers Regional Hospital immediately after surgical excision from patients, who had not received radiotherapy in the area or recent chemotherapy.^{31,32} Normal colon tissue was sampled from the same surgical specimens at a minimal distance of 10 cm from the macroscopic tumor border. The biopsies were placed in ice-cold advanced DMEM/F12 medium (Gibco, Denmark) with 1% GlutaMAX (ThermoFisher, Denmark) and kept on ice during transport to the Department of Biomedicine at Aarhus University, Denmark.

The human biopsy collection was designed to ensure that the sampling did not influence the surgical procedure or standard diagnostic workup.

2.2 | Mouse tissue

Murine breast cancer was induced by overexpression of the neu (ErbB2/HER2) proto-oncogene in FVB/N-Tg(MMTVneu)202Mul/J mice, which results in palpable tumor development when the mice are around 6 months of age.^{33,34} After mice were sacrificed by cervical dislocation, surgical biopsies of breast cancer tissue and normal breast tissue were immediately sampled and transferred to cold physiological saline solution.

2.3 | Freshly isolated breast organoids

From the human and murine breast biopsies, we freshly isolated organoids by partial enzymatic digestion using collagenase type 3. The tissue samples were first cut into 1 mm pieces in phosphate-buffered saline and then transferred to Tissue Culture Flat Tubes (Techno

FIGURE 1 Resting intracellular Ca^{2+} levels and responses to ATP, UTP and cyclopiazonic acid (CPA) are elevated in murine breast cancer compared with normal breast tissue. (A) Images of Fura-2-loaded organoids freshly isolated from murine normal breast tissue (left panel) and breast cancer tissue (right panel). The images are shown at the same magnification; the scale bar represents 50 μm . (B) Original traces showing ATP- and CPA-induced intracellular Ca^{2+} dynamics in organoids isolated from murine breast cancer and normal breast tissue. (C) Averaged baseline intracellular Ca^{2+} levels in organoids isolated from murine breast cancer and normal breast tissue ($n = 40\text{--}56$). The Ca^{2+} levels are expressed relative to the average value for the breast cancer tissue. (D) Average intracellular Ca^{2+} responses to ATP in organoids isolated from murine breast cancer and normal breast tissue ($n = 6\text{--}31$). Where indicated, the nonselective P2 receptor antagonist suramin (100 μM) was added. (E) Average ATP-induced intracellular Ca^{2+} responses in organoids from murine breast cancer and normal breast tissue at extracellular pH (pH_o) 7.4 and 6.8 ($n = 15$). (F) Original traces showing UTP-induced intracellular Ca^{2+} dynamics in organoids isolated from murine breast cancer and normal breast tissue. (G) Average intracellular Ca^{2+} responses to UTP in organoids isolated from murine breast cancer and normal breast tissue ($n = 8$). (H) Original traces showing UDP- and CPA-induced intracellular Ca^{2+} dynamics in organoids isolated from murine breast cancer and normal breast tissue. (I + J) Average intracellular Ca^{2+} responses to UDP (I, $n = 6$) and CPA (J, $n = 6$) in organoids isolated from murine breast cancer and normal breast tissue. (K) Original traces showing ATP- and benzoylbenzoyl (Bz)ATP-induced Ca^{2+} dynamics in murine breast cancer tissue. (L) Average intracellular Ca^{2+} responses to BzATP and ATP in organoids isolated from murine breast cancer and normal breast tissue ($n = 5$). In panel C, D, G, I, J and L, single parameters were compared between two groups by two-tailed Student's *t* test. In panel D, we tested for linear trend by one way ANOVA. In panel E, we tested the effect of two variables on a third variable by two-way ANOVA followed by Sidak's posttest. * $P < .05$; ** $P < .01$; *** $P < .001$, NS: not significantly different vs normal under similar conditions. # $P < .05$; ## $P < .001$ vs 100 μM ATP in Cancer. The Ca^{2+} responses are expressed relative to the average response of breast cancer organoids exposed to 100 μM ATP

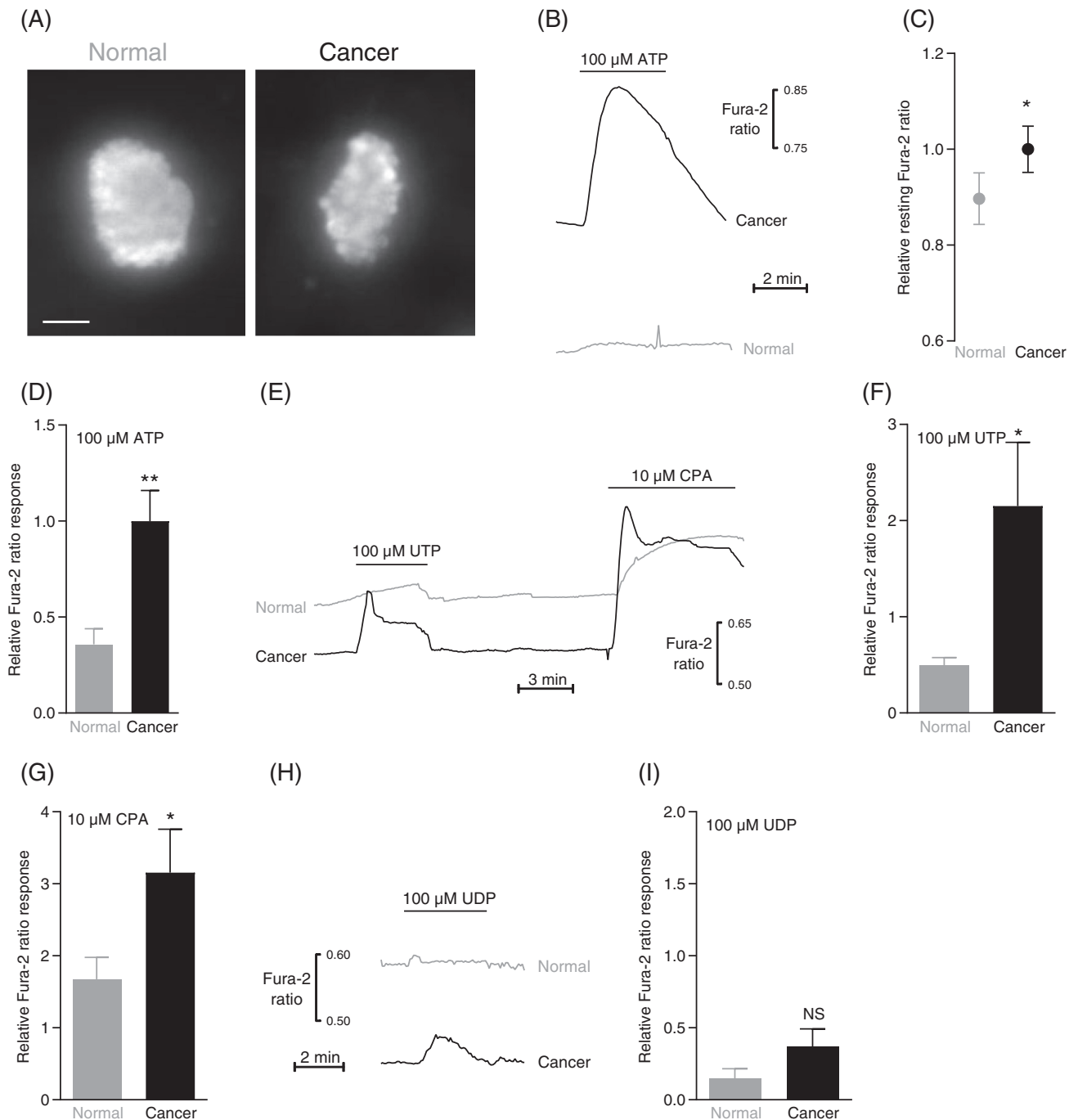


FIGURE 2 Resting intracellular Ca^{2+} levels and responses to ATP, UTP and cyclopiazonic acid (CPA) are elevated in human breast cancer compared with normal breast tissue. (A) Images of Fura-2-loaded organoids freshly isolated from human normal breast tissue (left panel) and breast cancer tissue (right panel). The images are shown at the same magnification; the scale bar represents 50 μm . (B) Original traces showing ATP-induced intracellular Ca^{2+} dynamics in organoids isolated from human breast cancer and normal breast tissue. (C) Average baseline intracellular Ca^{2+} levels in organoids isolated from breast cancer and matched normal breast tissue ($n = 33$). The Ca^{2+} levels are expressed relative to the average value for the breast cancer tissue. (D) Average intracellular Ca^{2+} responses to ATP in organoids isolated from human breast cancer and normal breast tissue ($n = 23$). (E) Original traces showing UTP- and CPA-induced intracellular Ca^{2+} dynamics in organoids isolated from human breast cancer and normal breast tissue. (F + G) Average intracellular Ca^{2+} responses to UTP (F, $n = 9$) and CPA (G, $n = 12$) in organoids isolated from human breast cancer and normal breast tissue. (H) Original traces showing UDP-induced intracellular Ca^{2+} dynamics in organoids isolated from human breast cancer and normal breast tissue. (I) Average intracellular Ca^{2+} responses to UDP in organoids from human breast cancer and normal breast tissue ($n = 8$). The data were compared by paired two-tailed Student's t test. * $P < .05$; ** $P < .01$, NS: not significantly different vs normal under similar conditions. The Ca^{2+} responses are expressed relative to the average response of breast cancer organoids exposed to 100 μM ATP

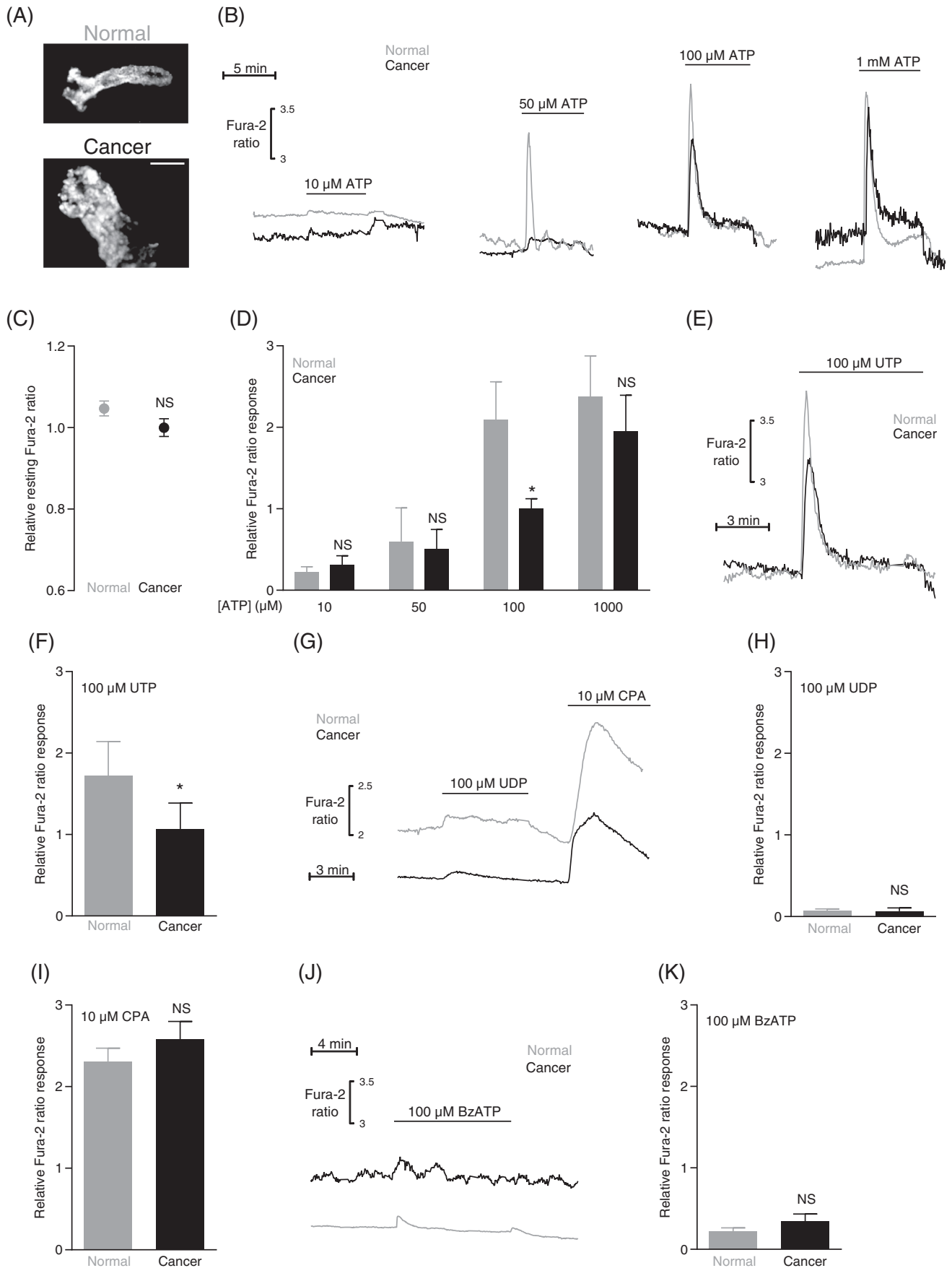


FIGURE 3 Legend on next page.

Plastic Products AG, Switzerland) containing advanced DMEM/F12 culture medium (Life Technologies, Denmark) added 10% fetal bovine serum (Biochrom AG, Germany), 1% GlutaMAX and 450 IU/mL collagenase type 3 (Worthington Biochemical Corporation, Lakewood, New Jersey). After continuous shaking overnight (human tissue) or for 4 h (mouse tissue) at 60 rpm in an incubator with 5% CO₂ at 37°C, the isolated organoids sedimented for 20 min by gravitational forces and were then used directly for experiments. We observed no signs of bacterial infection. The isolated organoids are multicellular conglomerates of approximately 150 μm diameter (Figures 1A and 2A), and we have previously shown that they are dominated by cytokeratin 19-positive epithelial cells with fewer smooth muscle α-actin-positive myofibroblasts.^{30,34,35} Although we cannot fully exclude that the enzymatic treatment influences extracellular epitopes and hence the function of membrane proteins, (a) the partial digestion was mild in order to generate organoids rather than single cell suspensions and (b) we have previously shown that—at least for acid-base transporters—functions evaluated in freshly isolated breast cancer organoids resemble those observed in slices of breast cancer tissue.^{29,30,34,36} We investigated the organoids immediately after enzymatic digestion without subsequent culture in order to avoid phenotypic changes. The organoids were classified as “normal” or “cancer” based on the location and macroscopic evaluation of the biopsy site. The subsequent standard pathological evaluation confirmed the malignancy of the tumor mass, as well as the presence of surrounding normal tissue with clear surgical margins. Still, we cannot fully exclude the possibility that the normal tissue could include smaller precancerous lesions.

2.4 | Freshly isolated human colon crypts

Human colon crypts were prepared as previously described^{32,37} by placing small samples of biopsy material in Ca²⁺-free Ringer solution (in mM: 125 NaCl, 5 KCl, 1 MgCl₂, 5 Na-pyruvate, 10 HEPES, 5 EDTA [free acid], 5 glucose; adjusted to pH 7.4 with NaOH) heated to 37°C in a water bath on a shaking table for 20 min. After vigorous shaking, the samples sedimented for 5 min before the supernatant was removed, and the pellet was washed three times in DMEM medium.

The human colon crypts (Figure 3A) were investigated functionally directly after isolation in order to best maintain their original phenotype.

2.5 | Intracellular Ca²⁺ recordings

Isolated organoids or crypts were loaded for 30 min with 5 μM of the Ca²⁺-sensitive fluorophore Fura-2-AM in a load mix containing dimethyl sulfoxide, Cremophor EL and Pluronic F127 (final concentrations: 0.04%, 0.0016% and 0.008%, respectively). Next, the organoids and crypts—sedimented as described above—were transferred in a small volume (~100 μL) to the glass coverslip bottom (#1.5/0.17 mm thickness; 88% to 92% light transmission at 340, 380 and 510 nm; Menzel Gläser, Thermo Scientific, USA) of a custom-built chamber and mechanically fixed under a nylon mesh (mesh count 250 in.⁻¹, thread diameter 40 μm), which was held in place by a perforated stainless steel ring attached to a stainless steel rod mounted on a micromanipulator. The porosity of the mesh ensures that solution and gas exchange occurs rapidly and transmission light illumination is sufficient for easy organoid and crypt identification. Heated water from a thermostatically controlled water bath circulated through the square metal base (14 × 14 cm) of the experimental chamber in order to maintain the pre-warmed buffer solutions at 37°C within the cylindrical sample-containing chamber insert (diameter 2 cm). All elements in contact with the experimental buffer solutions were constructed from stainless steel to ensure high heat conductivity and avoid contamination with heavy metals. Solution changes and addition of reagents were achieved by direct pipetting. Throughout experiments, we continuously aerated the stationary pre-gassed buffer solutions in the chamber with 5% CO₂/balance air through a fixed stainless steel tube.

The crypts and organoids were investigated by wide-field microscopy. The sample-holding chamber was placed on the XY stage of an Olympus IX70 inverted microscope coupled to an EasyRatioPro fluorescence imaging system (Photon Technology International, USA) or a Nikon Diaphot 200 inverted microscope equipped with an SRV or R1 CCD Retiga camera (QImaging, Canada) and VisiView software (Visitron systems, Germany). Under software control, light excitation at alternating wavelengths was achieved by directing a 75 W xenon

FIGURE 3 Intracellular Ca²⁺ responses to ATP and UTP are attenuated in human colon cancer tissue compared with normal colon tissue. (A) Images of Fura-2-loaded crypt-like structures from normal colon tissue (upper panel) and colon cancer tissue (lower panel). The images are shown at the same magnification; the scale bar represents 100 μm. (B) Original traces showing ATP-induced intracellular Ca²⁺ dynamics in crypts from colon cancer and normal colon tissue. (C) Average baseline intracellular Ca²⁺ levels in crypts from colon cancer and normal colon tissue (n = 38). The Ca²⁺ levels are expressed relative to the average value for the colon cancer tissue. (D) Average intracellular Ca²⁺ responses to ATP in crypts from colon cancer and normal colon tissue (n = 6-21). (E) Original traces showing UTP-induced intracellular Ca²⁺ dynamics in crypts from colon cancer and normal colon tissue. (F) Average intracellular Ca²⁺ responses to UTP in crypts from colon cancer and normal colon tissue (n = 14). (G) Original traces showing UDP- and cyclopiazonic acid (CPA)-induced intracellular Ca²⁺ dynamics in crypts from colon cancer and normal colon tissue. (H + I) Average intracellular Ca²⁺ responses to UDP (H, n = 4) or CPA (I, n = 38) in crypts from colon cancer and normal colon tissue. (J) Original traces showing benzoylbenzoyl (Bz)ATP-induced intracellular Ca²⁺ dynamics in crypts from colon cancer and normal colon tissue. (K) Average intracellular Ca²⁺ responses to BzATP in crypts from colon cancer and normal colon tissue (n = 5). The data in panel C, F, H and I were compared by paired two-tailed Student's *t* test. In panel D, data were compared by repeated measures two-way ANOVA followed by Sidak's posttest. **P* < .05, NS: not significantly different vs normal under similar conditions. The Ca²⁺ responses are expressed relative to the average response of colon cancer crypts exposed to 100 μM ATP

arc light beam through either a DeltaRAM X High Speed Random Access Monochromator system (Photon Technology International) or a dynamic Lambda 10-B filter wheel and IQ25-W SmartShutter system (Sutter Instruments, Novato, California). As the fluorescence excitation and emission light paths of the inverted microscopes enter and leave the chamber from below, the nylon mesh used to immobilize the tissue did not interfere with the Fura-2 imaging.

We extracted fluorescence emission signals collected at 510 nm from organoids or crypts and ambient background fluorescence signals from image regions without tissue. We used pixel binning 4 for breast organoids (resolution 344×256) and 8 for colonic crypts (resolution 174×130). From the background-subtracted signals recorded during alternating excitation at 340 nm (E_{340} ; exposure time 1500 ms) and 380 nm (E_{380} ; exposure time 1000 ms for breast organoids and 500 ms for colonic crypts), we then calculated Fura-2 fluorescence emission ratios as E_{340}/E_{380} . This approach follows the method by Gryniewicz et al,³⁸ with the exception that we did not calibrate to absolute intracellular Ca^{2+} concentrations. Calibration of the Fura-2 fluorescence signal would require estimates of maximal (R_{max}) and minimal (R_{min}) Fura-2 ratios, which is usually achieved by first adding the Ca^{2+} ionophore ionomycin and then stepping from a high Ca^{2+} concentration that saturates Fura-2 (R_{max}) to a Ca^{2+} -free solution with excess EGTA (R_{min}). Further steps to record wavelength-specific background signals, for instance, by adding Mn^{2+} to quench the indicator may be required.³⁹ Because pilot experiments showed that the signal-to-noise ratio for organoids and crypts deteriorates rapidly already during the initial ionomycin exposure and calibration steps, we instead quantified intracellular Ca^{2+} responses to agonist stimulation as the peak increases in the Fura-2 fluorescence emission ratio (ie, $(E_{340}/E_{380})_{peak} - (E_{340}/E_{380})_{baseline}$) during the first 120 s of agonist exposure. To ease comparison between experiments performed over an extended period of time and spanning hardware and lamp changes, we separately normalized the peak Fura-2 ratio responses within each experimental series to the average response of the cancer tissue to 100 μ M ATP. Similarly, we displayed baseline Fura-2 fluorescence emission ratios (E_{340}/E_{380}) normalized to the average baseline ratio in the cancer tissue.

Autofluorescence constituted approximately 15% of the increase in fluorescence over the ambient background signal upon Fura-2 loading. Thus, potential differences or changes in autofluorescence are unlikely to influence the Fura-2 ratio dynamics substantially.

The physiological salt solution for these experiments had the following composition (in mM): 10 HEPES, 115.9 NaCl, 2.82 KCl, 1.2 $MgSO_4$, 22 $NaHCO_3$, 1.18 KH_2PO_4 , 1.6 $CaCl_2$, 0.03 EDTA (free acid) and 5.5 glucose. As previously discussed elsewhere,⁴⁰ the buffer composition was chosen to best resemble normal plasma concentrations. The low concentration of EDTA was added for its antioxidant properties.⁴¹ The solutions were heated to 37°C, added 5 mM probenecid to inhibit fluorophore extrusion by organic anion transporters, and bubbled with 5% CO_2 /balance air for at least 20 min before pH was adjusted to 7.40 with NaOH. In a subset of experiments, the concentration of $NaHCO_3$ was lowered to 5.5 mM, through isosmolar substitution with NaCl, and pH was adjusted to 6.80 with NaOH.

2.6 | Cell proliferation and survival assays

For cell proliferation assays, breast organoids isolated from cancer and matched normal tissue incubated for 6 h with 10 μ M bromodeoxyuridine (BrdU; B23151, Invitrogen) at 37°C with or without nucleotides added to the medium. Incorporation of the thymidine analog BrdU into newly synthesized DNA allows for subsequent identification of dividing cells based on immunofluorescence imaging. After the BrdU incubation period, the medium was aspirated by three consecutive washes in phosphate-buffered saline (PBS, in mM: 138 NaCl, 2.6 KCl, 8.1 Na_2HPO_4 , 1.5 KH_2PO_4 , pH 7.4), and the organoids were fixed in 75% ethanol for 20 min. The fixative was then aspirated by a triple-wash with PBS, and the DNA denatured in 1 M HCl for 1 h at 37°C. After another triple-wash with PBS + 0.05% Tween-20, we blocked with 2% normal goat serum added to the same solution. Samples were next incubated with an anti-BrdU mouse monoclonal primary antibody (#5292, Cell Signaling, Danvers, Massachusetts; diluted 1:1000 in PBS/0.05% Tween-20/2% normal goat serum) for 30 min at 37°C. After additional thorough washing in PBS + 0.05% Tween-20, the organoids incubated with Alexa488-labeled donkey anti-mouse secondary antibody (#A21202, Invitrogen; diluted 1:1000 in PBS/0.05% Tween-20) in the dark at 37°C for 1 h. Nuclei were co-stained with SYTO16 (Life Technologies; diluted 1:1000 in PBS) at room temperature for 5 min. After a final thorough wash, the organoids were mounted under a cover slip, visualized with a Zeiss LSM510META confocal laser scanning microscope, and proliferation indices (BrdU-positive cells/SYTO16-positive nuclei) calculated for 3 different focal planes in each organoid using ImageJ software (NIH, Bethesda, Maryland).

For cell survival analysis, the isolated breast organoids were incubated for 2 h under control conditions or with ATP added to the medium, and then loaded with 4 μ M calcein-AM and 2 μ M ethidium homodimer-1 in phosphate-buffered saline (DMSO solvent <0.1%) for 30 min. Organoids were excited on a Zeiss LSM510META confocal microscope at 488 nm and emission light collected simultaneously at 515 nm (calcein) and 635 nm (ethidium homodimer-1). We calculated the ratio of cells positive for ethidium homodimer-1 relative to calcein for three different focal planes in each organoid using ImageJ software.

2.7 | Statistics

Data are given as mean \pm SEM; n equals number of patients or animals (ie, biological replicates). We compared single variables between two groups by two-tailed Student's *t* test and between more than two groups by one-way ANOVA followed by Dunnett's posttest or test for linear trend. We used two-way ANOVA followed by Sidak's posttest to evaluate effects of two variables on a third variable. If the initial distribution was right-skewed, the data were log-transformed prior to statistical testing. We considered *P*-values smaller than 0.05 statistically significant. Statistical analyses were performed with GraphPad Prism 9.3.0 software.

3 | RESULTS

We used human and murine biopsies of breast and colon cancer and matched normal tissue to evaluate intracellular Ca^{2+} dynamics and their consequences for proliferation and cell death. Studying cellular signaling in preparations that closely resemble the human clinical condition is crucial, and comparisons with relevant normal tissue help predict the potential of individual therapeutic targets.

3.1 | Intracellular Ca^{2+} levels, organellar Ca^{2+} storage and purinergic responses are elevated in murine breast cancer tissue

When immersed in standard physiological salt solution at pH 7.4, the resting intracellular Ca^{2+} level was raised (Figure 1B,C) in organoids freshly isolated from murine breast cancer tissue (Figure 1A, right panel) compared with organoids isolated from normal breast tissue (Figure 1A, left panel).

Extracellular ATP produced much stronger intracellular Ca^{2+} rises when applied to organoids from murine breast cancer tissue than normal breast tissue (Figure 1B,D). These ATP responses were fully inhibited by prior application of 100 μM of the nonselective P2 receptor antagonist suramin (Figure 1D). Although extracellular acidification attenuated the intracellular Ca^{2+} dynamics of breast cancer tissue (Figure 1E), the difference in ATP-induced Ca^{2+} responses between murine breast cancer and normal breast tissue observed at extracellular pH (pH_o) 7.4 was also evident at pH_o 6.8, which resembles the conditions in poorly vascularized regions of breast carcinomas.

Consistent with involvement of P2Y₂ and P2Y₄ receptors,⁴² responses of breast organoids to 100 μM UTP (Figure 1F,G) were of similar magnitude as those to 100 μM ATP (Figure 1B,D). UTP responses also showed marked augmentation in murine breast cancer tissue compared with normal breast tissue (Figure 1F,G). In contrast, the response to the P2Y₆ and P2Y₁₄ agonist UDP⁴² was of similar magnitude in murine breast cancer tissue and normal breast tissue (Figure 1H,I).

Enhanced metabotropic signaling in cancer cells could imply a change in the organellar Ca^{2+} storage mechanisms. As we and others have previously observed elevated expression of SERCA2 in breast cancer tissue and cells,^{6,7} we next evaluated the response to 10 μM cyclopiazonic acid (CPA) that inhibits the sarco-/endoplasmic reticulum Ca^{2+} ATPase (Figure 1B,H,J). Indeed, the organoids isolated from murine breast cancer tissue, on average, responded with a greater CPA-induced elevation in cytosolic Ca^{2+} concentration than organoids from matched normal breast tissue (Figure 1J).

Earlier studies suggest that P2X7 receptors play a role in breast cancer. Yet, we observed only a minimal change in intracellular Ca^{2+} concentration when we applied 100 μM of the P2X7-specific agonist benzoylbenzoyl (Bz)ATP to organoids isolated from murine breast cancer tissue (Figure 1K,L).

3.2 | Intracellular Ca^{2+} levels, organellar Ca^{2+} storage, and purinergic responses are elevated in human breast cancer tissue

Organoids isolated from human breast cancer tissue (Figure 2A) responded with Ca^{2+} dynamics that were very similar to those of organoids isolated from murine breast cancer tissue (compare Figures 1 and 2).

On average, the resting intracellular Ca^{2+} concentration was elevated in human breast cancer tissue compared with normal breast tissue (Figure 2B,C).

Supporting a role for P2Y₂ and P2Y₄ receptors,⁴² intracellular Ca^{2+} responses to UTP were at least as large as responses to ATP; and for both nucleotides, the rise in intracellular Ca^{2+} concentration was markedly elevated in the human breast cancer tissue compared with normal breast tissue (Figure 2B,D-F). In contrast, the Ca^{2+} response to UDP (Figure 2H,I) was of small magnitude compared with ATP (Figure 2D) and UTP (Figure 2F) confirming that P2Y₆ and P2Y₁₄ receptors are not of major importance.⁴²

The human tissue samples were mostly from invasive ductal carcinomas, less frequently from invasive lobular carcinomas, and in a few instances from rarer histological subtypes (Table 1). When divided between the separate experimental series, the number of samples of each histological subtype was too small for

TABLE 1 Clinical and pathological patient characteristics of the breast cancer patients investigated in the current study

| | |
|--|------------|
| Number of patients | 33 |
| Patient age (years; median, interquartile range) | 62 (52-71) |
| Tumor size (mm; median, interquartile range) | 14 (12-19) |
| Histological type | |
| Invasive ductal carcinomas | 24 (73%) |
| Invasive lobular carcinomas | 6 (18%) |
| Other | 3 (9%) |
| HER2 receptor status | |
| Normal | 28 (85%) |
| Overexpression or gene amplification | 5 (15%) |
| Estrogen receptor status | |
| Positive | 31 (94%) |
| Negative | 2 (6%) |
| Malignancy grade | |
| I | 4 (12%) |
| II | 20 (61%) |
| III | 9 (27%) |
| Axillary lymph node status | |
| Negative | 18 (55%) |
| Positive | 15 (45%) |

Note: Other histological types include combined invasive ductal and lobular carcinoma and apocrine carcinoma.

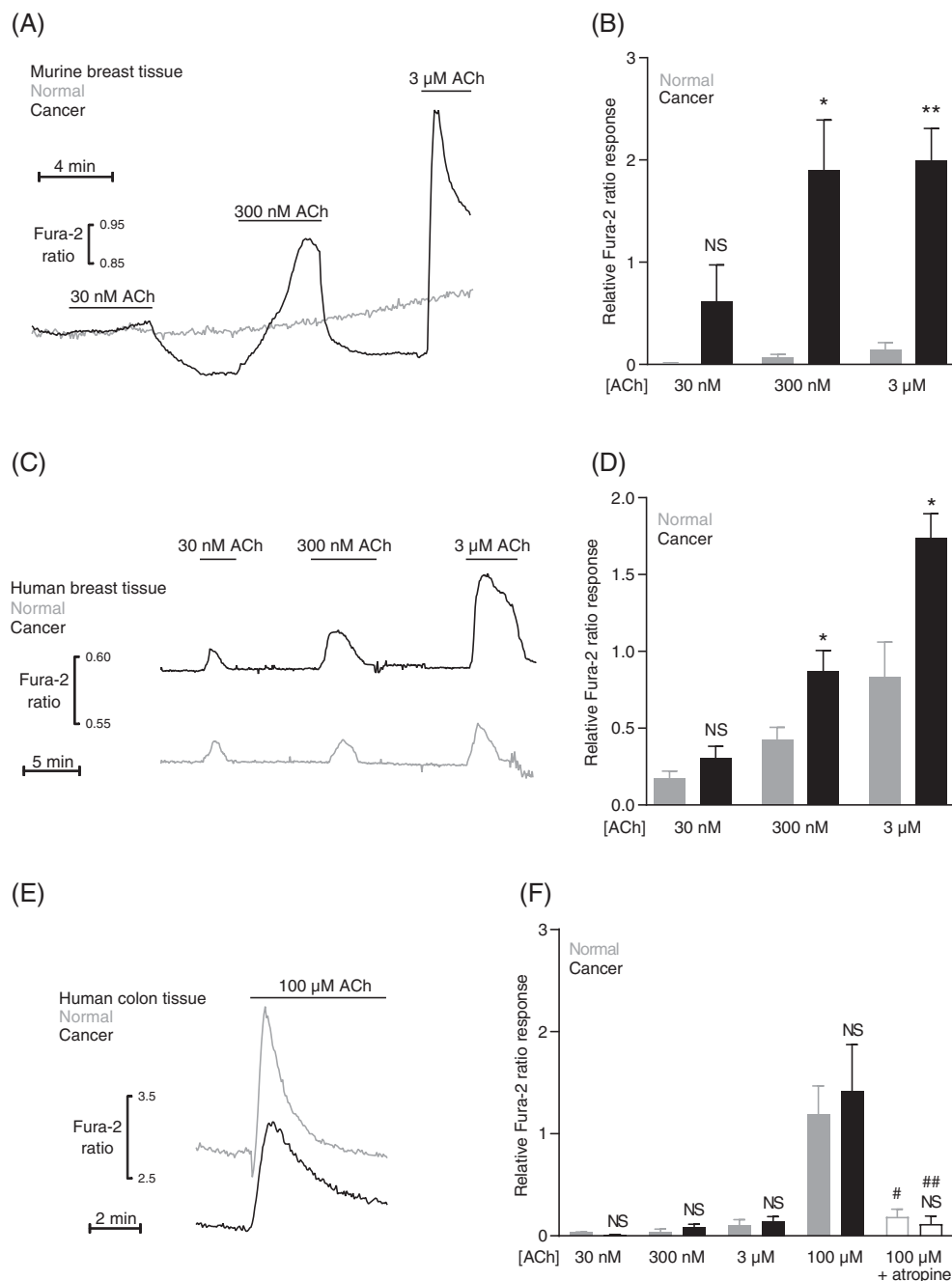
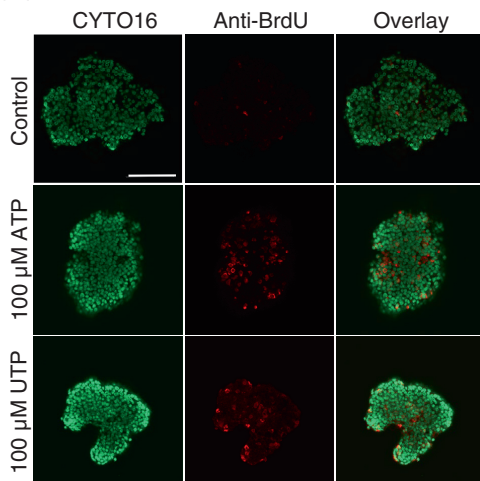


FIGURE 4 Acetylcholine (ACh)-induced intracellular Ca²⁺ responses are strongly augmented in human and murine breast cancer tissue compared with normal breast tissue. In contrast, acetylcholine-induced intracellular Ca²⁺ responses are unaffected in human colon cancer compared with normal colon tissue. (A-D) Original traces (A,C) and corresponding quantifications (B,D) of intracellular Ca²⁺ responses to acetylcholine in organoids isolated from murine (A,B) and human (C,D) breast cancer and normal breast tissue (n = 6-13). The Ca²⁺ responses are expressed relative to the average increase in Ca²⁺ concentration in breast cancer organoids when exposed to 100 μM ATP. (E + F) Original traces (E) and corresponding quantifications (F) of intracellular Ca²⁺ responses to acetylcholine in crypts from human colon cancer and normal colon tissue (n = 5-13). The Ca²⁺ responses are expressed relative to the average response of colon cancer crypts exposed to 100 μM ATP. The muscarinic receptor antagonist atropine was applied at a concentration of 1 μM. The data were compared by repeated measures two-way ANOVA followed by Sidak's posttest. *P < .05; **P < .01, NS: not significantly different vs normal under similar conditions. #P < .05; ##P < .01 vs 100 μM in tissue of same source (cancer or normal)

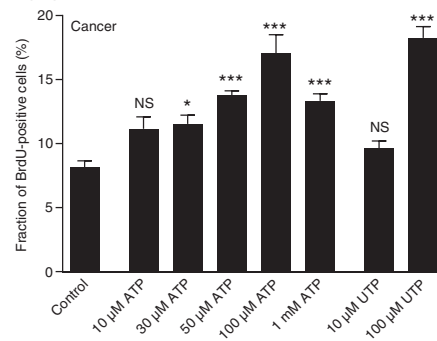
stratification and detailed analysis of how tumor heterogeneity influences Ca²⁺-responses. Still, our current evidence suggests that breast cancer tissue across the most common

histopathologies respond with enhanced ATP-induced intracellular Ca²⁺ elevations: the relative Fura-2 ratio response to 100 μM ATP was 0.47 ± 0.31 higher in lobular carcinomas than in

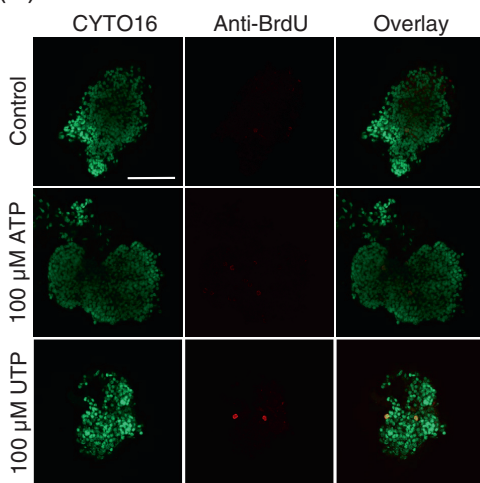
(A) Cancer



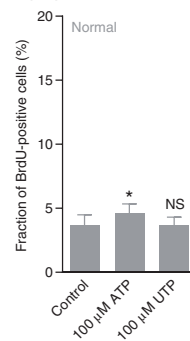
(B)



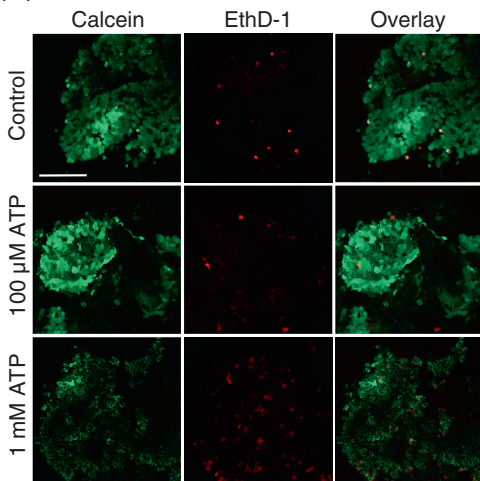
(C) Normal



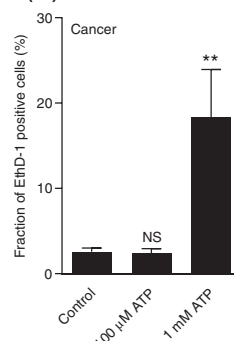
(D)



(E) Cancer



(F)

**FIGURE 5** ATP and UTP

promote cell proliferation in breast cancer tissue with minimal effect in normal breast tissue. In contrast, ATP induces cell death only when applied at very high concentration. (A-D) Representative images (A,C) and corresponding quantifications (B,D) of bromodeoxyuridine (BrdU) incorporation in organoids freshly isolated from breast cancer tissue (A,B) and normal breast tissue (C,D). The organoids ($n = 5-6$) were incubated with BrdU for 6 h under control conditions or with ATP or UTP present at the indicated concentrations. All images are shown at the same magnification; the scale bars represent 100 μm . (E + F) Representative images (E) and corresponding quantifications (F) of cell death in freshly isolated breast cancer organoids stained with calcein and ethidium homodimer-1 (EthD-1). The isolated organoids ($n = 4$) were evaluated after a 2-h control period or following incubation with ATP at the indicated concentration. All images are shown at the same magnification; the scale bar represents 100 μm . Data were compared by one-way ANOVA followed by Dunnett's posttest. * $P < .05$; ** $P < .01$; *** $P < .001$; NS: not significantly different vs control

matching normal tissue ($n = 3$) with corresponding values of 0.74 ± 0.21 for ductal carcinomas ($n = 17$) and 0.39 ± 0.13 for mixed ductal and lobular carcinomas ($n = 2$).

Consistent with augmented organellar Ca^{2+} stores, the rise in Ca^{2+} concentration during application of 10 μM CPA was greater in human breast cancer tissue than in matched normal breast tissue (Figure 2E,G).

3.3 | Intracellular Ca²⁺ levels and organellar Ca²⁺ storage are unaltered whereas purinergic responses are attenuated in human colon cancer tissue

In order to explore whether the observed changes in human and murine breast cancer tissue (Figures 1 and 2) are observed also in other solid cancers, we next evaluated Ca²⁺ dynamics in human colon cancer compared with normal colon tissue (Figure 3). Consistent with our previous observations,³² the crypt-like structures isolated from human colon cancer tissue (Figure 3A, lower panel) were wider and more irregular than the crypts isolated from normal colon tissue (Figure 3A, upper panel).

In the human colon cancer tissue, we found no evidence for an elevated resting Ca²⁺ level (Figure 3B,C). In contrast to our observations from the breast cancer tissue (Figures 1 and 2), responses to ATP were attenuated—especially around the 100 μM range—in crypts isolated from human colon cancer compared with normal colon tissue (Figure 3B,D). Similarly, the intracellular Ca²⁺ response to 100 μM UTP was markedly reduced in human colon cancer tissue compared with normal colon tissue (Figure 3E,F). These findings are consistent with altered P2Y₂ and P2Y₄ receptor signaling⁴²; and indeed, we observed almost no change of the intracellular Ca²⁺ concentration in human colon cancer or normal colon tissue when we stimulated P2Y₆ and P2Y₁₄ receptors with UDP (Figure 3G,H).

Although attenuated intracellular Ca²⁺ responses to P2Y₂ and P2Y₄ receptor activation could suggest a change in the capacity of the organellar Ca²⁺ stores, this is an unlikely explanation for the colon cancer tissue because we find no difference in the Ca²⁺ responses elicited by 10 μM CPA between colon cancer tissue and normal colon tissue (Figure 3G,I).

We observed only a small intracellular Ca²⁺ response in colon cancer tissue as well as in normal colon tissue when we stimulated P2X₇ receptors with BzATP (Figure 3J,K).

3.4 | Acetylcholine responses are enhanced in human and murine breast cancer tissue but unaffected in human colon cancer tissue

As described above, inhibition of the sarco-/endoplasmic reticulum Ca²⁺ ATPase elicits enhanced Ca²⁺ responses in breast cancer tissue compared with normal breast tissue (Figures 1J and 2G). This difference was not observed between colon cancer tissue and normal colon tissue (Figure 3I). Together these observations imply that the intracellular Ca²⁺ stores are magnified specifically during breast carcinogenesis. The observations moreover suggest that G_{α(q/11)}-coupled metabotropic receptor agonists in addition to nucleotides will induce greater Ca²⁺ responses in breast cancer tissue but not in colon cancer tissue when compared with corresponding normal tissue. In order to test this hypothesis, we next applied acetylcholine to organoids isolated from breast cancer and normal breast tissue (Figure 4A–D) as well as to crypts isolated from colon cancer and normal colon tissue (Figure 4E,F). Acetylcholine induced markedly greater elevations in

intracellular Ca²⁺ concentration in organoids from both murine (Figure 4A,B) and human (Figure 4C,D) breast cancer tissue compared with normal breast tissue. In sharp contrast, acetylcholine-induced increases in intracellular Ca²⁺ concentration were comparable for crypts isolated from colon cancer tissue and normal colon tissue (Figure 4E,F). The dependency of the acetylcholine responses on muscarinic receptors was confirmed by their full inhibition following incubation with 1 μM atropine (Figure 4F).

3.5 | Purinergic signals increase proliferation in breast cancer tissue

We next tested whether the greater Ca²⁺ responses elicited by extracellular nucleotides in the breast cancer tissue relative to normal breast tissue associate with an altered proliferative activity (Figure 5A–D). We studied cell proliferation by BrdU incorporation for 6 h and found that ATP concentration-dependently elevated the proportion of dividing cells in the breast cancer tissue (Figure 5A,B). We observed a much smaller effect of 100 μM ATP on cell proliferation in the normal breast tissue (Figure 5C,D) consistent with the smaller ATP-induced Ca²⁺ responses (Figure 1D). In further agreement with the magnitude of the intracellular Ca²⁺ responses (Figure 1G), UTP elevated cell proliferation in breast cancer tissue (Figure 5A,B) but showed no significant effect in normal breast tissue (Figure 5C,D). At the highest tested concentration (1 mM)—that exceeds reported values from solid cancer tissue^{22–24}—the pro-proliferative effect of ATP appeared to wane in the breast cancer tissue (Figure 5B).

3.6 | Purinergic signals cause cell death in breast cancer tissue only at very high nucleotide concentrations

Given the tendency for declining cell proliferation at very high nucleotide concentrations (Figure 5B), we hypothesized that ATP at millimolar concentrations can induce cell death. Indeed, whereas we observed no effect of 100 μM ATP on the fraction of dead cells, we saw widespread cell death when the breast cancer tissue was stimulated with 1 mM ATP (Figure 5E,F).

4 | DISCUSSION

The chemical microenvironment in solid tumors shapes cancer development and progression and responses to anti-cancer therapies. A striking characteristic of solid cancer tissue—beyond hypoxia and acidosis—is elevated nucleotide concentrations^{22–24} that arise from a shifted balance between controlled cellular release through large anion-conducting membrane pores or exocytosis, escape of cellular content during necrosis, cellular uptake via macropinocytosis and enzymatic conversion by ectonucleotidases.^{43–45}

The implications of the chemical tumor microenvironment for cancer and stromal cell functions are only starting to emerge; and in the current study, we show that nucleotide-induced responses acquired during carcinogenesis promote cell proliferation in breast cancer tissue (Figure 5A-D). The identified drastic differences in cellular Ca^{2+} handling (Figures 1-4) between breast and colon cancer tissue and corresponding normal tissue support a promising new therapeutic avenue for targeting malignant development and progression.

The intense acidity of the tumor microenvironment^{6,46} is particularly interesting in the context of this study because ATP, Ca^{2+} and H^+ homeostasis are interlinked by multiple mechanisms: Ca^{2+} ATPases transport H^+ as counter ions and may thereby alter pH reciprocally in neighboring intracellular compartments or between the cytosol and extracellular space.⁴ Associated net ATP hydrolysis also liberates H^+ ; however, under steady-state conditions, H^+ consumption during ATP synthesis is expected to balance H^+ release from ATP hydrolysis avoiding substantial acute changes in intracellular pH (pH_i).⁴⁷ Because H^+ and Ca^{2+} buffers overlap and pH modifies the activity of many Ca^{2+} transporters and channels, changes in pH_i have potential to modify the intracellular Ca^{2+} concentration.⁴ Interestingly, local acid-base conditions may moreover influence macropinocytosis, which is commonly inhibited by amiloride-derivatives that block Na^+/H^+ exchangers.⁴⁸⁻⁵¹ Macropinocytosis is prominent in breast and colon cancer cells,⁴⁹⁻⁵¹ and could accelerate cellular ATP uptake.⁴³

In breast and colon cancer tissue, we find that intracellular Ca^{2+} responses to UTP are equal to or greater than responses to ATP whereas UDP has only minimal effect (Figures 1-3). This Ca^{2+} response pattern is indicative of predominant P2Y_2 and P2Y_4 signaling.⁴² Compared with matching normal tissue, the responses to ATP and UTP are strongly elevated in human and murine breast cancer tissue (Figures 1 and 2) but attenuated in human colon cancer tissue (Figure 3). The influence of P2Y_2 receptors on proliferation is controversial in cultured breast cancer cell lines: in estrogen receptor-positive MCF7 cells and triple-negative MDA-MB-231 cells derived from human breast adenocarcinomas, activation of P2Y_2 receptors has been found to have little to no effect on proliferation,⁵² to increase proliferation,⁵³ or to suppress proliferation.⁵⁴ It is not clear whether these reported inconsistencies in proliferative activity relate to variation in cell culture conditions or other experimental circumstances. In the current study—based on acute functional investigations of breast biopsies—ATP and UTP both stimulate cell proliferation in breast cancer tissue (Figure 5A,B) but show no major influence on proliferation in normal breast tissue (Figure 5C,D).

Previous studies reported a combination of pro- and anti-neoplastic consequences of purinergic signaling.¹ We confirm here that extracellular nucleotides can accelerate cell proliferation (Figure 5A-D) but also enhance cell death (Figure 5E,F). However, whereas nucleotides at 30 to 100 μM concentration enhance proliferation, they stimulate cell death only when elevated to the millimolar range, which is higher than typically observed in solid cancer tissue.²²⁻²⁴ Thus, our findings support that the increased purinergic

signaling reported for solid cancer tissue will mainly promote neoplastic progression in the breast.

The observed pattern of purinergic signaling—with amplified Ca^{2+} responses in breast but not colon cancer tissue (Figures 1-3)—extends also to activation of other metabotropic receptors. Whereas acetylcholine induces strongly augmented Ca^{2+} responses in breast cancer tissue compared with normal breast tissue (Figure 4A-D), acetylcholine responses in colon cancer tissue are very similar to those of normal colon tissue (Figure 4E,F). This is particularly interesting because the different responsiveness between breast and colon cancer tissue is consistent with the magnitude of their Ca^{2+} response when the sarco-/endoplasmic reticulum Ca^{2+} ATPase is inhibited with CPA (Figures 1J, 2G and 3I). Hence, our findings suggest that intracellular Ca^{2+} signals downstream of metabotropic receptors are shaped by the capacity of the intracellular Ca^{2+} stores. Consistent with the enhanced store release responses of breast cancer tissue (Figures 1J and 2G), we and others previously found that SERCA2 protein expression levels are elevated in breast cancer tissue and cell lines compared with normal breast tissue and nontumorigenic cells.^{6,7}

Expression of SERCA in organellar membranes allows cancer cells to lower cytosolic Ca^{2+} levels acutely. However, by augmenting organellar Ca^{2+} storage at the expense of extrusion across the plasma membrane, elevated SERCA activity also amplifies the capacity for subsequent Ca^{2+} release in response to metabotropic receptor agonists such as extracellular nucleotides or acetylcholine. In addition to changes in Ca^{2+} store release capacity, it is possible that Ca^{2+} responses of cancer cells are influenced by expressional changes or posttranslational modifications that alter the activity of purinergic and cholinergic receptors during carcinogenesis. Several studies report high expression of purinergic receptors in breast and colon cancer cell lines,^{44,55} but poor specificity of antibodies for quantification of purinergic receptor expression is a challenge,⁵⁶ and more work is needed to establish the molecular pathways that determine the magnitude of nucleotide-induced Ca^{2+} responses in cancer cells.

P2X7 receptors have previously been implicated in breast malignancy.^{57,58} However, based on Ca^{2+} responses of minimal magnitude to BzATP (Figures 1K,L and 3J,K), we conclude that P2X7 receptors do not contribute substantively to nucleotide-induced intracellular Ca^{2+} responses in breast or colon cancer tissue.

In contrast to previous studies based primarily on cancer cell lines, the current investigations employ freshly isolated tissue from humans and mice. We obtain very consistent results between human and murine breast cancer tissue (Figures 1, 2 and 4), which is in congruence with our earlier studies of acid-base parameters, where findings from carcinogen- and ErbB2-induced models of murine breast carcinogenesis extrapolated well to human breast cancer tissue.^{30,34,35} We previously showed that acid-base parameters recorded in organoids freshly isolated from human breast cancer tissue can predict proliferative activity and metastasis.³⁶ Our current investigation shows that acutely isolated breast organoids and colon crypts can be used for evaluating intracellular Ca^{2+} dynamics (Figures 1-4) and study consequences for cell proliferation and survival (Figure 5). Based on our collective previous and current work, the approach of studying freshly

isolated human and murine tissue preparations—that retain a profile accurately reflecting the clinical condition—is very well suited for evaluating carcinogenesis-related adaptations and for screening pharmacological agents for functional activity.

Notably, differences between normal and cancer tissue may exist for a number of reasons: individual cell types can change phenotype, for instance, due to mutations or adaptations to the microenvironment, or the relative distribution of cell types can change due to selection and expansion of cells with a survival or proliferative benefit under the tumor conditions. Irrespectively, the comparison of organoids and crypts freshly isolated from human and murine cancer tissue to matched normal tissue provides a unique approach for studying carcinogenesis-related functional differences with potential for pharmacological targeting.

In conclusion, we find that intracellular Ca^{2+} signaling varies dramatically between breast and colon cancer. Resting intracellular Ca^{2+} concentrations, organellar Ca^{2+} storage, and responses to ATP, UTP and acetylcholine are elevated in breast cancer tissue compared with normal breast tissue. Accordingly, ATP and UTP strikingly stimulate proliferation in breast cancer tissue, yet only minimally enhance proliferation in normal breast tissue. We observe increases in cell death only when ATP concentrations are above the expected pathophysiological range. These studies support that changes in Ca^{2+} signaling acquired during carcinogenesis shape cancer cell phenotypes and, in particular, that elevated nucleotide concentrations have overall pro-malignant consequences in breast cancer tissue.

AUTHOR CONTRIBUTIONS

Boedtkjer conceived of the studies and designed the overall experimental approach. Mele, Hauerslev, Dabir, Balling, Pedersen, Vahl, Johansen, Tramm and Christiansen collected tissue and performed the clinical and pathological evaluations. Henningsen (colonic crypt and organoid Ca^{2+} fluorimetry; proliferation and survival), McWhan (organoid Ca^{2+} fluorimetry), Dam (human organoid Ca^{2+} fluorimetry) and Voss (proliferation) performed the experiments. Henningsen (colonic crypt Ca^{2+} fluorimetry; organoid proliferation and survival), McWhan (organoid Ca^{2+} fluorimetry), Dam (human organoid Ca^{2+} fluorimetry) and Boedtkjer designed the experimental protocols, analyzed and interpreted the results. Boedtkjer drafted the manuscript. All authors edited the manuscript and approved the final version. The work reported in the paper has been performed by the authors, unless clearly specified in the text.

ACKNOWLEDGEMENTS

The authors would like to express gratitude to the patients, who participated in the studies. We also thank the doctors and nurses—particularly Drs. Jens J. Christiansen and Ida E. Holm—who assisted with sampling of human tissue at Regionshospitalet Randers and Aarhus University Hospital, Denmark.

FUNDING INFORMATION

This study was financially supported by the Danish Cancer Society (R146-A9461 to Boedtkjer; R127-A8262-15-S7 to Henningsen) and the Independent Research Fund Denmark (7025-00050B to Boedtkjer).

CONFLICT OF INTEREST

The authors declare no conflict of interest.

DATA AVAILABILITY STATEMENT

Anonymized data from this study are available from the corresponding author upon reasonable request.

ETHICS STATEMENT

Human breast tissue biopsies: The Mid-Jutland Regional Committee on Health Research Ethics approved the human breast tissue sampling (No. M-20100288). Breast cancer patients gave written informed consent. The Danish Data Protection Agency approved the procedures for data handling (No. 1-16-02-191-16). **Human colon tissue biopsies:** The Mid-Jutland Regional Committee on Health Research Ethics approved the procedure for human colon tissue sampling and concluded that written informed consent was not required according to Danish legislation, because the studies involved excess surgically resected tissue and all postsurgical tissue and data handling was anonymized (enquiry no. 157/2014). **Murine experiments:** The Danish Animal Experiments Inspectorate approved the mouse experiments (2012-15-2935-00002 and 2012-15-2934-00103).

ORCID

Ebbe Boedtkjer  <https://orcid.org/0000-0002-5078-9279>

REFERENCES

- Burnstock G, di Virgilio F. Purinergic signalling and cancer. *Purinergic Signal*. 2013;9:491-540.
- Diaz-Ruiz R, Rigoulet M, Devin A. The Warburg and Crabtree effects: on the origin of cancer cell energy metabolism and of yeast glucose repression. *Biochim Biophys Acta Bioenerg*. 2011;1807:568-576.
- Varghese E, Samuel SM, Sadiq Z, et al. Anti-cancer agents in proliferation and cell death: the calcium connection. *Int J Mol Sci*. 2019;20:3017.
- Boedtkjer E. Ion channels, transporters, and sensors interact with the acidic tumor microenvironment to modify cancer progression. *Rev Physiol Biochem Pharmacol*. 2022;182:39-84.
- Monteith GR, McAndrew D, Faddy HM, Roberts-Thomson SJ. Calcium and cancer: targeting Ca^{2+} transport. *Nat Rev Cancer*. 2007;7:519-530.
- Voss NCS, Dreyer T, Henningsen MB, Vahl P, Honoré B, Boedtkjer E. Targeting the acidic tumor microenvironment: unexpected pro-neoplastic effects of oral NaHCO_3 therapy in murine breast tissue. *Cancers (Basel)*. 2020;12:891.
- Christodoulou P, Yiallouris A, Michail A, Christodoulou MI, Politis PK, Patrikios I. Altered SERCA expression in breast cancer. *Medicina (Kaunas)*. 2021;57:1074.
- Gélébart P, Kovács T, Brouland JP, et al. Expression of endomembrane calcium pumps in colon and gastric cancer cells. Induction of SERCA3 expression during differentiation. *J Biol Chem*. 2002;277:26310-26320.
- Brouland JP, Gélébart P, Kovács T, Enouf J, Grossmann J, Papp B. The loss of sarco/endoplasmic reticulum calcium transport ATPase 3 expression is an early event during the multistep process of colon carcinogenesis. *Am J Pathol*. 2005;167:233-242.
- Ohkubo T, Yamazaki J. T-type voltage-activated calcium channel $\text{Ca}_v3.1$, but not $\text{Ca}_v3.2$, is involved in the inhibition of proliferation and apoptosis in MCF-7 human breast cancer cells. *Int J Oncol*. 2012;41:267-275.

11. Zhang S, Miao Y, Zheng X, et al. STIM1 and STIM2 differently regulate endogenous Ca^{2+} entry and promote TGF- β -induced EMT in breast cancer cells. *Biochem Biophys Res Commun.* 2017;488:74-80.
12. McAndrew D, Grice DM, Peters AA, et al. ORAI1-mediated calcium influx in lactation and in breast cancer. *Mol Cancer Ther.* 2011;10:448-460.
13. Faouzi M, Hague F, Potier M, Ahidouch A, Sevestre H, Ouidid-Ahidouch H. Down-regulation of Orai3 arrests cell-cycle progression and induces apoptosis in breast cancer cells but not in normal breast epithelial cells. *J Cell Physiol.* 2011;226:542-551.
14. Weiss H, Amberger A, Widschwendter M, Margreiter R, Ofner D, Dietl P. Inhibition of store-operated calcium entry contributes to the anti-proliferative effect of non-steroidal anti-inflammatory drugs in human colon cancer cells. *Int J Cancer.* 2001;92:877-882.
15. Jackisch C, Hahm HA, Tombal B, et al. Delayed micromolar elevation in intracellular calcium precedes induction of apoptosis in thapsigargin-treated breast cancer cells. *Clin Cancer Res.* 2000;6:2844-2850.
16. Jaskulska A, Janecka AE, Gach-Janczak K. Thapsigargin-from traditional medicine to anticancer drug. *Int J Mol Sci.* 2020;22:4.
17. Mahalingam D, Peguero J, Cen P, et al. A phase II, multicenter, single-arm study of mipsagargin (G-202) as a second-line therapy following sorafenib for adult patients with progressive advanced hepatocellular carcinoma. *Cancers (Basel).* 2019;11:833.
18. Abdoul-Azize S, Buquet C, Li H, Picquetot JM, Vannier JP. Integration of Ca^{2+} signaling regulates the breast tumor cell response to simvastatin and doxorubicin. *Oncogene.* 2018;37:4979-4993.
19. Baggott RR, Mohamed TM, Oceandy D, et al. Disruption of the interaction between PMCA2 and calcineurin triggers apoptosis and enhances paclitaxel-induced cytotoxicity in breast cancer cells. *Carcinogenesis.* 2012;33:2362-2368.
20. Pan Z, Avila A, Gollahon L. Paclitaxel induces apoptosis in breast cancer cells through different calcium-regulating mechanisms depending on external calcium conditions. *Int J Mol Sci.* 2014;15:2672-2694.
21. Zhou Y, Tozzi F, Chen J, et al. Intracellular ATP levels are a pivotal determinant of chemoresistance in colon cancer cells. *Cancer Res.* 2012;72:304-314.
22. Pellegatti P, Raffaghello L, Bianchi G, Piccardi F, Pistoia V, di Virgilio F. Increased level of extracellular ATP at tumor sites: in vivo imaging with plasma membrane luciferase. *PLoS One.* 2008;3:e2599.
23. Michaud M, Martins I, Sukkurwala AQ, et al. Autophagy-dependent anticancer immune responses induced by chemotherapeutic agents in mice. *Science.* 2011;334:1573-1577.
24. Falzoni S, Donvito G, di Virgilio F. Detecting adenosine triphosphate in the pericellular space. *Interface Focus.* 2013;3:20120101.
25. Burnstock G. Purine and purinergic receptors. *Brain Neurosci Adv.* 2018;2:2398212818817494.
26. McClatchey AI, Yap AS. Contact inhibition (of proliferation) redux. *Curr Opin Cell Biol.* 2012;24:685-694.
27. Russo P, del Bufalo A, Milic M, Salinaro G, Fini M, Cesario A. Cholinergic receptors as target for cancer therapy in a systems medicine perspective. *Curr Mol Med.* 2014;14:1126-1138.
28. Mucchietto V, Crespi A, Fasoli F, Clementi F, Gotti C. Neuronal acetylcholine nicotinic receptors as new targets for lung cancer treatment. *Curr Pharm des.* 2016;22:2160-2169.
29. Boedtker E, Moreira JM, Mele M, et al. Contribution of Na^+ , HCO_3^- -cotransport to cellular pH control in human breast cancer: a role for the breast cancer susceptibility locus NBCn1 (SLC4A7). *Int J Cancer.* 2013;132:1288-1299.
30. Lee S, Mele M, Vahl P, Christiansen PM, Jensen VED, Boedtker E. Na^+ , HCO_3^- -cotransport is functionally upregulated during human breast carcinogenesis and required for the inverted pH gradient across the plasma membrane. *Pflugers Arch.* 2015;467:367-377.
31. Voss NCS, Kold-Petersen H, Boedtker E. Enhanced nitric oxide signaling amplifies vasorelaxation of human colon cancer feed arteries. *Am J Physiol Heart Circ Physiol.* 2019;316:H245-H254.
32. Voss NCS, Kold-Petersen H, Henningsen MB, Homilius C, Boedtker E. Upregulated Na^+ / H^+ -exchange protects human colon cancer tissue against intracellular acidification. *Biomed Res Int.* 2019;2019:3702783.
33. Guy CT, Webster MA, Schaller M, Parsons TJ, Cardiff RD, Muller WJ. Expression of the neu protooncogene in the mammary epithelium of transgenic mice induces metastatic disease. *Proc Natl Acad Sci U S A.* 1992;89:10578-10582.
34. Lee S, Axelsen TV, Jessen N, Pedersen SF, Vahl P, Boedtker E. Na^+ , HCO_3^- -cotransporter NBCn1 (Slc4a7) accelerates ErbB2-induced breast cancer development and tumor growth in mice. *Oncogene.* 2018;37:5569-5584.
35. Lee S, Axelsen TV, Andersen AP, Vahl P, Pedersen SF, Boedtker E. Disrupting Na^+ , HCO_3^- -cotransporter NBCn1 (Slc4a7) delays murine breast cancer development. *Oncogene.* 2016;35:2112-2122.
36. Toft NJ, Axelsen TV, Pedersen HL, et al. Acid-base transporters and pH dynamics in human breast carcinomas predict proliferative activity, metastasis, and survival. *Elife.* 2021;10:e68447.
37. Sørensen MV, Strandsby AB, Larsen CK, Praetorius HA, Leipziger J. The secretory $\text{K}_{\text{Ca}}1.1$ channel localises to crypts of distal mouse colon: functional and molecular evidence. *Pflugers Arch.* 2011;462:745-752.
38. Gryniewicz G, Poenie M, Tsien RY. A new generation of Ca^{2+} indicators with greatly improved fluorescence properties. *J Biol Chem.* 1985;260:3440-3450.
39. Jensen PE, Mulvany MJ, Aalkjaer C, Nilsson H, Yamaguchi H. Free cytosolic Ca^{2+} measured with Ca^{2+} -selective electrodes and fura 2 in rat mesenteric resistance arteries. *Am J Physiol.* 1993;265:H741-H746.
40. Boedtker E, Aalkjaer C. The solution to bicarbonate. *Am J Physiol Heart Circ Physiol.* 2022;322:H685-H686.
41. Nedergaard OA, Vagne A, Bevan JA. Effect of the chelating agents, EDTA, 2,2'-bipyridine, 8-hydroxyquinoline and pyrophosphoric acid, on norepinephrine uptake by rabbit aorta. *J Pharmacol Exp Ther.* 1968;163:136-146.
42. Jacobson KA, Paoletta S, Katritch V, et al. Nucleotides acting at P2Y receptors: connecting structure and function. *Mol Pharmacol.* 2015;88:220-230.
43. Qian Y, Wang X, Liu Y, et al. Extracellular ATP is internalized by macropinocytosis and induces intracellular ATP increase and drug resistance in cancer cells. *Cancer Lett.* 2014;351:242-251.
44. de Araújo JB, Kerkhoff VV, de Oliveira Maciel SFV, de Resende ESDT. Targeting the purinergic pathway in breast cancer and its therapeutic applications. *Purinergic Signal.* 2021;17:179-200.
45. Taruno A. ATP release channels. *Int J Mol Sci.* 2018;19:808.
46. Vaupel P, Kallinowski F, Okunieff P. Blood flow, oxygen and nutrient supply, and metabolic microenvironment of human tumors: a review. *Cancer Res.* 1989;49:6449-6465.
47. Boedtker E. Na^+ , HCO_3^- cotransporter NBCn1 accelerates breast carcinogenesis. *Cancer Metastasis Rev.* 2019;38:165-178.
48. Koivusalo M, Welch C, Hayashi H, et al. Amiloride inhibits macropinocytosis by lowering submembranous pH and preventing Rac1 and Cdc42 signaling. *J Cell Biol.* 2010;188:547-563.
49. Ramachandran S, Sennoune SR, Sharma M, et al. Expression and function of SLC38A5, an amino acid-coupled Na^+ / H^+ exchanger, in triple-negative breast cancer and its relevance to macropinocytosis. *Biochem J.* 2021;478:3957-3976.
50. Zhu BY, Shang BY, Du Y, et al. A new HDAC inhibitor cinnamoylphenazine shows antitumor activity in association with intensive macropinocytosis. *Oncotarget.* 2017;8:14748-14758.

51. Delpout S, Sisson G, Black KM, Richardson CD. Measles virus enters breast and colon cancer cell lines through a PVRL4-mediated macropinocytosis pathway. *J Virol*. 2017;91:e02191-16.
52. Chadet S, Jelassi B, Wannous R, et al. The activation of P2Y₂ receptors increases MCF-7 breast cancer cells migration through the MEK-ERK1/2 signalling pathway. *Carcinogenesis*. 2014;35:1238-1247.
53. Jin H, Eun SY, Lee JS, et al. P2Y₂ receptor activation by nucleotides released from highly metastatic breast cancer cells increases tumor growth and invasion via crosstalk with endothelial cells. *Breast Cancer Res*. 2014;16:R77.
54. Li HJ, Wang LY, Qu HN, et al. P2Y₂ receptor-mediated modulation of estrogen-induced proliferation of breast cancer cells. *Mol Cell Endocrinol*. 2011;338:28-37.
55. Dillard C, Borde C, Mohammad A, et al. Expression pattern of purinergic signaling components in colorectal cancer cells and differential cellular outcomes induced by extracellular ATP and adenosine. *Int J Mol Sci*. 2021;22:11472.
56. Yu W, Hill WG. Lack of specificity shown by P2Y₆ receptor antibodies. *Naunyn Schmiedebergs Arch Pharmacol*. 2013;386:885-891.
57. Park M, Kim J, Phuong NTT, et al. Involvement of the P2X7 receptor in the migration and metastasis of tamoxifen-resistant breast cancer: effects on small extracellular vesicles production. *Sci Rep*. 2019;9:11587.
58. Xia J, Yu X, Tang L, Li G, He T. P2X7 receptor stimulates breast cancer cell invasion and migration via the AKT pathway. *Oncol Rep*. 2015;34:103-110.

How to cite this article: Henningsen MB, McWhan K, Dam VS, et al. Amplified Ca²⁺ dynamics and accelerated cell proliferation in breast cancer tissue during purinergic stimulation. *Int J Cancer*. 2022;151(7):1150-1165. doi:[10.1002/ijc.34147](https://doi.org/10.1002/ijc.34147)